Element Polarization Selection Optimization for Radar Clutter Suppression via Mixed-Integer Programming

JIAHENG WANG
YALONG WANG
XUEJING ZHANG
ZISHU HE, Senior Member, IEEE
JUN LI
University of Electronic Science and Technology of China, Chengdu, China

The information of the target in the polarization domain helps to solve the problem of low-speed target detection. However, due to the limitation of hardware complexity, polarimetric radar usually configures only one radio frequency (RF) channel for each polarized antenna. Therefore, for the problem of clutter suppression, it is necessary to design the element polarization of the transmitter and receiver under such constraints. In this article, we analyze the problem of single-end element polarization selection optimization and the joint polarization optimization of transmitter and receiver with the constraint that the polarized antenna has only one RF channel. We first give the signal model of the polarization-sensitive array based on the polarization scattering mechanism, and then present the optimization model for polarization optimization. The corresponding optimization problem is the fractional quadratic programming with the binary integer constraint, and a heuristic algorithm based on the alternating direction method of multipliers frame is proposed to find a solution to the mixed-integer programming. Numerical simulation results show that although the convergence of the algorithm cannot be guaranteed, we can use this algorithm to find a suboptimal solution in a short time, and the output signal-to-clutter plus noise ratio is improved compared to the single-polarimetric radar.

Received 26 June 2024; revised 20 October 2024 and 29 December 2024; accepted 9 January 2025. Date of publication 13 January 2025; date of current version 11 June 2025.

DOI. No. 10.1109/TAES.2025.3529426

Refereeing of this contribution was handled by C. Clemente.

This work was supported in part by the National Natural Science Foundation of China under Grant 62031007 and Grant 62101101, in part by the Sichuan Science and Technology Program under Grant 2024NSFSC1433, and in part by the Peng Cheng Shang Xue Education Fund under Grant XY2021602.

Authors' address: Jiaheng Wang, Yalong Wang, Xuejing Zhang, Zishu He, and Jun Li are with the School of Information and Communication Engineering, University of Electronic Science and Technology of China, Chengdu 611731, China, E-mail: (xjzhang7@163.com). *(Corresponding author: Xuejing Zhang.)*

I. INTRODUCTION

Polarization is a kind of important information that radar can use in addition to the information in the time and spatial domains [1]. Since the polarization state of the received signal is not only related to the polarization state of the signal radiated by the transmitter, it is also affected by the shape, size, attitude, material, and other factors of the target, we can use appropriate signal processing methods to fully mine and utilize the polarization information, thereby improving the performance of the polarimetric radar.

It is worth noting that polarization-sensitive arrays are the basis for sensing polarization information, and there are many research results based on various forms of polarization-sensitive arrays: the authors in [2], [3], [4], and [5] proposed the estimation method of the direction-of-arrival (DOA) and the polarization parameter based on the vector antenna, which is a complete electromagnetic sensor that consists of three orthogonal dipoles and three orthogonal current loops with a common phase center, and the orthogonal relationship between the Poynting vector and the electromagnetic field is used for the parameter estimation.

However, due to the mutual coupling of array elements, this kind of polarization-sensitive array is difficult to apply in engineering, and the widely used polarization-sensitive array is composed of the orthogonal dipole pairs; therefore, the radar data of the HH channel, VV channel, and the HV (or VH) channel [6], [7] are assumed available for signal processing. There are signal processing methods for parameter estimation [8], [9], [10], [11], anti-interference/clutter [12], [13], [14], adaptive detection [15], [16], [17], [18], [19], [20], [21], [22], [23], and target classification and identification [24], [25], [26], [27], [28], [29]. Moreover, there are techniques, such as polarimetric calibration [30], [31], [32] and polarization isolation [33], [34], [35], to improve the reliability of the polarimetric radar system.

But limited by the hardware system complexity, the polarized antenna is equipped with only one radio frequency (RF) channel in practical applications, and therefore, the polarimetric radar cannot transmit or receive horizontally polarized and vertically polarized signals simultaneously, instead, it will transmit (or receive) signals in horizontal or vertical polarization alternately or it will use two radars with different polarization to obtain the polarimetric radar data. This prompts us to make further simplifications on the basis of this kind of array such that the polarization information can be used more concisely.

Recently, the polarization-sensitive array composed of single but differently polarized antennas has caught the attention of researchers, and the received signal of such an array has been proven to contain information in the polarization domain. The method of DOA estimation [36],

[37], [38], adaptive beamforming [39], and adaptive detection [40] for this kind of array has been analyzed to improve the ability to suppress the main lobe jammer and detect the low-speed target.

The polarization sensing capabilities of the single but differently polarized antenna array and limitations of the polarimetric radar in practical applications motivate us to consider that for the array composed of the cross dipoles, we can use different array elements to transmit (or receive) the horizontally and vertically polarized signals separately, thereby improving the output signal-to-clutter plus noise ratio (SCNR) of the radar compared to the single-polarimetric radar.

To solve the above problem, in this article, we first present the transmitting and receiving signal model of the polarization-sensitive array based on the polarization scattering mechanism. Then, to maximize the output SCNR after adaptive filtering, optimization models are given for situations, such as transmitter (or receiver) polarization optimization and the joint polarization optimization of transmitter and receiver. Moreover, a heuristic algorithm based on the alternating direction method of multipliers (ADMM) frame is proposed to find a suboptimal solution to the mixed-integer programming. Finally, through numerical simulations, we verify that the optimized transceiver polarization can improve the output SCNR.

Notations: Throughout this article, we use lightface for scalar a, lower case boldface for vector $\mathbf{a}$, and upper case boldface for matrix $\mathbf{A}$. $(\cdot)^T$, $(\cdot)^H$, $\otimes$, $||\cdot||$, and $\mathbb{E}(\cdot)$ denote the transpose, conjugate transpose, Kronecker product, norm, and expectation operators, respectively. $\mathbf{R}^{-1}$ represents the inverse of $\mathbf{R}$, $\mathbf{I}_L$ denotes the identity matrix with dimension L, and diag$(\cdot)$ and bdiag$(\cdot)$ represent the operation of the diagonal matrix and the block-diagonal matrix, respectively.

II. SIGNAL MODEL

We consider a uniform linear array with M polarized antennas, and each antenna can transmit (or receive) the horizontal and vertical components of the polarized signal. For the point-like target, the polarimetric scattering matrix [41] is given by

$$\mathbf{S} = \begin{bmatrix} s_{hh} & s_{hv} \\ s_{vh} & s_{vv} \end{bmatrix}. \tag{1}$$

The subscripts "h" and "v" denote the transmitting and receiving polarizations, e.g., s_{hv} describes the proportion of vertically transmitted waves returning horizontally to the antenna. The transmitting–scattering–receiving process of polarized signals is expressed as

$$x = \mathbf{e}_0^T \mathbf{S} \mathbf{t}_0 \tag{2}$$

where $\mathbf{e}_0 = [e_{h,0}, e_{v,0}]^T$ and $\mathbf{t}_0 = [t_{h,0}, t_{v,0}]^T$ represent the receive and transmit polarization vector, respectively. In this article, we consider that each polarized antenna is equipped with only one RF channel, and only one polarization channel can be selected for transmission or reception. Therefore, the above two variables satisfy $\mathbf{e}_0 \in \{0, 1\}^2$, $e_{h,0} + e_{v,0} = 1$ and $\mathbf{t}_0 \in \{0, 1\}^2$, $t_{h,0} + t_{v,0} = 1$.

Furthermore, a burst of N pulses is transmitted during a coherent processing interval, and the pulse repetition frequency is f_r. Hence, there are $L = MN$ samples that are received for a given range cell; note that the transmitting and receiving polarization can be different in different pulses. Under the target-presence hypothesis, the received signal $\mathbf{x} \in \mathbb{C}^{L\times 1}$ contains multiple components, i.e.,

$$\mathbf{x} = \mathbf{x}_{\text{tgt}} + \mathbf{x}_c + \mathbf{n} \tag{3}$$

where $\mathbf{n}$ is the Gaussian white noise with mean zero and variance σ^2. We assume each of the antenna transmits orthogonal waveforms; therefore, the lth sample of the target component (denoted as $\mathbf{x}_{\text{tgt}}(l)$) is

$$\mathbf{x}_{\text{tgt}}(l) = (\mathbf{e}_l^T \mathbf{S}_{\text{tgt}} \mathbf{t}_l)\mathbf{p}_{\text{st}}(l),\ l = 1, 2, \ldots, L \tag{4}$$

where $\mathbf{p}_{st} = \mathbf{p}_s \otimes \mathbf{p}_t$ is the spatial–Doppler steering vector, and

$$\mathbf{S}_{\text{tgt}} = \begin{bmatrix} s_{hh}^{\text{tgt}} & s_{hv}^{\text{tgt}} \\ s_{vh}^{\text{tgt}} & s_{vv}^{\text{tgt}} \end{bmatrix} \tag{5}$$

is the scattering matrix for the target. Note the following equation relationship:

$$\mathbf{e}_l^T \mathbf{S}_{\text{tgt}} \mathbf{t}_l = \mathbf{e}_l^T \mathbf{T}_l \mathbf{s}_{\text{tgt}} \tag{6}$$

where

$$\mathbf{s}_{\text{tgt}} = [s_{hh}, s_{vv}, s_{hv}]^T \tag{7}$$

and

$$\mathbf{T}_l = \begin{bmatrix} t_{h,l} & 0 & t_{v,l} \\ 0 & t_{v,l} & t_{h,l} \end{bmatrix}. \tag{8}$$

Therefore, the target component is denoted as

$$\mathbf{x}_{\text{tgt}} = \mathbf{E}\mathbf{T}\mathbf{b}_{\text{tgt}} \tag{9}$$

where $\mathbf{b}_{\text{tgt}} = \mathbf{p}_{st} \otimes \mathbf{s}_{\text{tgt}}$, $\mathbf{T} = \text{bdiag}(\mathbf{T}_1, \mathbf{T}_2, \ldots, \mathbf{T}_L) \in \mathbb{R}^{2L\times 3L}$, and $\mathbf{E} = \text{bdiag}(\mathbf{e}_1^T, \mathbf{e}_2^T, \ldots, \mathbf{e}_L^T) \in \mathbb{R}^{L\times 2L}$, i.e., $\mathbf{T}$ and $\mathbf{E}$ are block diagonal matrices with $\mathbf{T}_1, \mathbf{T}_2, \ldots, \mathbf{T}_L$ and $\mathbf{e}_1^T, \mathbf{e}_2^T, \ldots, \mathbf{e}_L^T$ as diagonal blocks, respectively.

Similarly, the clutter component $\mathbf{x}_c$ in the received signal is

$$\mathbf{x}_c = \mathbf{E}\mathbf{T}\sum_{i=1}^{N_c} \mathbf{p}_{\text{st},i} \otimes \mathbf{s}_{c,i} = \mathbf{E}\mathbf{T}\sum_{i=1}^{N_c} \mathbf{b}_{c,i} \tag{10}$$

where N_c is the number of clutter patches, and $\mathbf{b}_{c,i} = \mathbf{p}_{\text{st},i} \otimes \mathbf{s}_{c,i}$ is the polarization-space–time steering vector of the ith clutter patch. Assuming that $\mathbf{s}_{c,i}$ are independent and identically distributed, and due to the independence between the polarization characteristic and the space–time characteristic, we have

$$\mathbb{E}\left[\left(\sum_{i=1}^{N_c} \mathbf{p}_{\text{st},i} \otimes \mathbf{s}_{c,i}\right)\left(\sum_{i=1}^{N_c} \mathbf{p}_{\text{st},i} \otimes \mathbf{s}_{c,i}\right)^H\right]$$
$$= \mathbb{E}\left[\sum_{i=1}^{N_c} \xi_i \mathbf{p}_{\text{st},i}\mathbf{p}_{\text{st},i}^H\right] \otimes \mathbb{E}\left[\sum_{i=1}^{N_c} \mathbf{s}_{c,i}\mathbf{s}_{c,i}^H\right]$$

$$= \mathbf{R}_{st} \otimes \mathbf{R}_p \tag{11}$$

where the space–time covariance matrix (CM) is $\mathbf{R}_{\text{st}} \in \mathbb{C}^{L\times L}$, ξ_i is the power of the ith clutter patch, and the polarimetric CM is given by

$$\mathbf{R}_p = \begin{bmatrix} 1 & \rho_c\sqrt{\gamma_c} & 0 \\ \rho_c^*\sqrt{\gamma_c} & \gamma_c & 0 \\ 0 & 0 & \delta_c \end{bmatrix} \tag{12}$$

where δ_c is the power ratio between the HV and HH channels, γ_c the power ratio between the VV and HH channels, and ρ_c the correlation between the HH and VV channels.[1] Therefore, the clutter and noise CM is

$$\begin{aligned} \mathbf{R}_{cn} &= \mathbb{E}\left[(\mathbf{x}_c + \mathbf{n})(\mathbf{x}_c + \mathbf{n})^H\right] \\ &= \mathbf{ET}(\mathbf{R}_{\text{st}} \otimes \mathbf{R}_p)\mathbf{T}^H\mathbf{E}^H + \sigma^2\mathbf{I}_L. \end{aligned} \tag{13}$$

Based on the above signal model, the output SCNR is easily obtained as

$$\text{SCNR} = \frac{\mathbf{w}^H\mathbf{R}_{\text{tgt}}\mathbf{w}}{\mathbf{w}^H\mathbf{R}_{\text{cn}}\mathbf{w}} \tag{14}$$

where $\mathbf{R}_{\text{tgt}} = \mathbf{ETb}_{\text{tgt}}\mathbf{b}_{\text{tgt}}^H\mathbf{T}^H\mathbf{E}^H$ and $\mathbf{w}$ is the filter weight. If the minimum variance distortionless response criterion is adopted, we have

$$\mathbf{w} = \frac{\mathbf{R}_{\text{cn}}^{-1}\mathbf{ETb}_{\text{tgt}}}{\mathbf{b}_{\text{tgt}}^H\mathbf{T}^H\mathbf{E}^H\mathbf{R}_{\text{cn}}^{-1}\mathbf{ETb}_{\text{tgt}}} \tag{15}$$

and therefore, the output SCNR is

$$\text{SCNR} = \mathbf{b}_{\text{tgt}}^H\mathbf{T}^H\mathbf{E}^H\mathbf{R}_{\text{cn}}^{-1}\mathbf{ETb}_{\text{tgt}}. \tag{16}$$

From (13) and (16), we can see that the transmitter polarization (i.e., $\mathbf{T}$) and the receiver polarization (i.e., $\mathbf{E}$) will influence the output SCNR; therefore, how to design the transmitter polarization and/or receiver polarization to maximize the output SCNR has become an issue worth considering. We will investigate this issue in the rest of this article.

III. PROBLEM FORMULATION

In this section, we will discuss the problem of polarization optimization. In detail, the problem of transmitter (or receiver) polarization optimization and the problem of joint polarization optimization are considered, respectively.

A. Transmitter/Receiver Polarization Optimization

We first consider the problem of transmitter (or receiver) polarization optimization, and from (14), we have

$$\text{SCNR} = \frac{\mathbf{w}^H\mathbf{ETb}_{\text{tgt}}\mathbf{b}_{\text{tgt}}^H\mathbf{T}^H\mathbf{E}^H\mathbf{w}}{\mathbf{w}^H\mathbf{ET}(\mathbf{R}_{\text{st}} \otimes \mathbf{R}_p)\mathbf{T}^H\mathbf{E}^H\mathbf{w} + \sigma^2\|\mathbf{w}\|^2}. \tag{17}$$

[1]Here, we assume that the polarimetric CM has the form of reflection symmetry. Note that the CM depends on the geometry of the observed target as well as the radar look angle, and readers can refer to [42], [43], and [44] for other possible structures.

Note that the following identity transformation can be deployed:

$$\mathbf{w}^H\mathbf{ET} = \mathbf{t}^T\mathbf{\Omega} = \mathbf{e}^T\mathbf{\Psi} \tag{18}$$

where we have

$$\begin{aligned} \mathbf{t} &= [\mathbf{t}_1^T, \mathbf{t}_2^T, \ldots, \mathbf{t}_L^T]^T \in \mathbb{R}^{2L\times 1} \\ \mathbf{e} &= [\mathbf{e}_1^T, \mathbf{e}_2^T, \ldots, \mathbf{e}_L^T]^T \in \mathbb{R}^{2L\times 1} \\ \mathbf{\Omega} &= \text{bdiag}(\mathbf{\Omega}_1, \mathbf{\Omega}_2, \ldots, \mathbf{\Omega}_L) \in \mathbb{C}^{2L\times 3L} \\ \mathbf{\Omega}_l &= \begin{bmatrix} w_l^* e_{h,l} & 0 & w_l^* e_{v,l} \\ 0 & w_l^* e_{v,l} & w_l^* e_{h,l} \end{bmatrix} \end{aligned} \tag{19}$$

i.e., $\mathbf{\Omega}$ is the block diagonal matrix with $\mathbf{\Omega}_1, \mathbf{\Omega}_2, \ldots, \mathbf{\Omega}_L$ as diagonal blocks and $\mathbf{\Psi} = \text{diag}(\mathbf{w}^* \otimes \mathbf{1}_2)\mathbf{T} \in \mathbb{C}^{2L\times 2L}$. Therefore, the output SCNR can be reshaped as

$$\begin{aligned} \text{SCNR} &= \frac{\mathbf{t}^T\mathbf{\Omega}\mathbf{b}_{\text{tgt}}\mathbf{b}_{\text{tgt}}^H\mathbf{\Omega}^H\mathbf{t}}{\mathbf{t}^T\mathbf{\Omega}(\mathbf{R}_{\text{st}} \otimes \mathbf{R}_p)\mathbf{\Omega}^H\mathbf{t} + \sigma^2\|\mathbf{w}\|^2} \\ &= \frac{\mathbf{e}^T\mathbf{\Psi}\mathbf{b}_{\text{tgt}}\mathbf{b}_{\text{tgt}}^H\mathbf{\Psi}^H\mathbf{e}}{\mathbf{e}^T\mathbf{\Psi}(\mathbf{R}_{\text{st}} \otimes \mathbf{R}_p)\mathbf{\Psi}^H\mathbf{e} + \sigma^2\|\mathbf{w}\|^2}. \end{aligned} \tag{20}$$

Note that $\mathbf{\Omega}$ depends on $\mathbf{e}$ and $\mathbf{w}$, and $\mathbf{\Psi}$ depends on $\mathbf{t}$ and $\mathbf{w}$, respectively. We take the minimization of the reciprocal of SCNR (i.e., the maximization of SCNR) as the objective function; since $||\mathbf{t}||^2 = ||\mathbf{e}||^2 = L$, the problem of transmitter polarization optimization can be presented as

$$\begin{aligned} \min_{\mathbf{t},\mathbf{w}} \quad & \frac{\mathbf{t}^T(\mathbf{\Omega}(\mathbf{R}_{\text{st}} \otimes \mathbf{R}_p)\mathbf{\Omega}^H + \sigma^2\|\mathbf{w}\|^2/L * \mathbf{I}_{2L})\mathbf{t}}{\mathbf{t}^T\mathbf{\Omega}\mathbf{b}_{\text{tgt}}\mathbf{b}_{\text{tgt}}^H\mathbf{\Omega}^H\mathbf{t}} \\ \text{s.t.} \quad & (\mathbf{I}_L \otimes \mathbf{1}_2^T)\mathbf{t} = \mathbf{1}_L \\ & \mathbf{t} \in \{0, 1\}^{2L}. \end{aligned} \tag{21}$$

As for the problem of receiver polarization optimization, it is denoted as

$$\begin{aligned} \min_{\mathbf{e},\mathbf{w}} \quad & \frac{\mathbf{e}^T(\mathbf{\Psi}(\mathbf{R}_{\text{st}} \otimes \mathbf{R}_p)\mathbf{\Psi}^H + \sigma^2\|\mathbf{w}\|^2/L * \mathbf{I}_{2L})\mathbf{e}}{\mathbf{e}^T\mathbf{\Psi}\mathbf{b}_{\text{tgt}}\mathbf{b}_{\text{tgt}}^H\mathbf{\Psi}^H\mathbf{e}} \\ \text{s.t.} \quad & (\mathbf{I}_L \otimes \mathbf{1}_2^T)\mathbf{e} = \mathbf{1}_L \\ & \mathbf{e} \in \{0, 1\}^{2L}. \end{aligned} \tag{22}$$

The above analysis is an optimization of one end, and the polarization of the other end is fixed. Then, we discuss the problem of joint polarization optimization of the transmitter and receiver.

B. Joint Polarization Optimization

The influence of transmitter polarization and the influence of receiver polarization on the output SCNR are reflected in $\mathbf{E}$ and $\mathbf{T}$, respectively. According to (16), we define $\mathbf{Q} = \mathbf{ET}$, and this variable reflects the impact of the joint polarization of the transmitter and receiver on the output SCNR.

Therefore, we use $\mathbf{Q} \in \mathbb{R}^{L\times 3L}$ as the object to analyze the impact of joint polarization, and $\mathbf{Q}$ is equal to the product of the receiver polarization matrix $\mathbf{E} \in \mathbb{R}^{L\times 2L}$ and the transmitter polarization matrix $\mathbf{T} \in \mathbb{R}^{2L\times 3L}$. We observe that $\mathbf{Q}$ is a block diagonal matrix with $\mathbf{q}_1^T, \mathbf{q}_2^T, \ldots, \mathbf{q}_L^T$ as

diagonal blocks, i.e.,

$$\mathbf{Q} = \text{bdiag}(\mathbf{q}_1^T, \mathbf{q}_2^T, \ldots, \mathbf{q}_L^T) \in \mathbb{R}^{L\times 3L} \tag{23}$$

where we have $\mathbf{q}_l = [e_{h,l}t_{h,l}, e_{v,l}t_{v,l}, e_{h,l}t_{v,l} + e_{v,l}t_{h,l}]^T \in \mathbb{R}^{3\times 1}$, and

$$\mathbf{q}_l = \begin{cases} [1,0,0]^T, e_{h,l}=1, t_{h,l}=1 \\ [0,0,1]^T, e_{h,l}=0, t_{h,l}=1 \\ [0,0,1]^T, e_{h,l}=1, t_{h,l}=0 \\ [0,1,0]^T, e_{h,l}=0, t_{h,l}=0 \end{cases}, l = 1,2,\ldots,L. \tag{24}$$

We can see that $\mathbf{q}_l$, $l = 1, 2, \ldots, L$, have a corresponding relationship with different transceiver polarization combinations, and we can achieve the joint optimization of transmitter and receiver polarization by optimizing this variable.

Therefore, the problem of joint polarization optimization is cast as

$$\begin{aligned} \min_{\mathbf{q},\mathbf{w}} \quad & \frac{\mathbf{q}^T(\mathbf{W}(\mathbf{R}_{\text{st}}\otimes\mathbf{R}_p)\mathbf{W}^H + \sigma^2\|\mathbf{w}\|^2/L * \mathbf{I}_{3L})\mathbf{q}}{\mathbf{q}^T\mathbf{W}\mathbf{b}_{\text{tgt}}\mathbf{b}_{\text{tgt}}^H\mathbf{W}^H\mathbf{q}} \\ \text{s.t.} \quad & (\mathbf{I}_L\otimes\mathbf{1}_3^T)\mathbf{q} = \mathbf{1}_L \\ & \mathbf{q}\in\{0,1\}^{3L} \end{aligned} \tag{25}$$

where $\mathbf{q} = [\mathbf{q}_1^T, \ldots, \mathbf{q}_l^T, \ldots, \mathbf{q}_L^T]^T \in \mathbb{R}^{3L\times 1}$, and $\mathbf{W} = \text{diag}(\mathbf{w}^* \otimes \mathbf{1}_3) \in \mathbb{C}^{3L\times 3L}$. After completing the solution, the optimal transmitter and receiver polarization can be obtained through the relationship shown in (24).

Note that the optimization problems in (21), (22), and (25) have the following form:

$$\begin{aligned} \min_{\mathbf{y},\mathbf{w}} \quad & \frac{\mathbf{y}^T\mathbf{\Phi}(\mathbf{w})\mathbf{y}}{\mathbf{y}^T\mathbf{\Gamma}(\mathbf{w})\mathbf{y}} \\ \text{s.t.} \quad & \mathbf{A}\mathbf{y} = \mathbf{b} \\ & \mathbf{y}\in\{0,1\}^{N_pL} \end{aligned} \tag{26}$$

where $\mathbf{\Gamma}(\mathbf{w})$ is a rank-one matrix, $\mathbf{A} = \mathbf{I}_L \otimes \mathbf{1}_{N_p}^T$, and $\mathbf{b} = \mathbf{1}_L$. For different problems, $\mathbf{\Phi}(\mathbf{w})$ and $\mathbf{\Gamma}(\mathbf{w})$ have different values. Moreover, $N_p = 2$ for optimization problem in (21) and (22), and $N_p = 3$ for optimization problem in (25). Next, we will achieve polarization optimization by discussing the solution to this problem.

IV. POLARIZATION OPTIMIZATION BASED ON ADMM

In this section, we first analyze the gains that polarization optimization can bring, and then investigate the solution of optimization problems in (26). For the latter one, we first discuss some possible problem-solving methods and analyze limitations faced by these methods, then an iterative method, which is based on the ADMM frame, is proposed to obtain a solution.

A. Performance Analysis

Xie et al. [14] analyzed the gain that the dual-polarimetric radar can achieve in the problem of clutter suppression compared with the single-polarimetric radar. In this section, we first give the performance analysis for the polarization optimization.

As shown in Appendix, the output SCNR in (16) can be given as

$$\text{SCNR} \approx \frac{\left\|\tilde{\mathbf{b}}_{\text{tgt}}\right\|^2}{\sigma^2}\left(1 - \frac{\tilde{\mathbf{b}}_{\text{tgt}}^H\tilde{\mathbf{V}}_{pst}(\tilde{\mathbf{V}}_{pst}^H\tilde{\mathbf{V}}_{pst})^{-1}\tilde{\mathbf{V}}_{pst}^H\tilde{\mathbf{b}}_{\text{tgt}}}{\left\|\tilde{\mathbf{b}}_{\text{tgt}}\right\|^2}\right) \tag{27}$$

where we have $\tilde{\mathbf{b}}_{\text{tgt}} = \mathbf{Q}\mathbf{b}_{\text{tgt}}$, $\mathbf{Q}(\mathbf{R}_{\text{st}}\otimes\mathbf{R}_p)\mathbf{Q}^H = \tilde{\mathbf{V}}_{pst}^H\tilde{\mathbf{\Lambda}}_{pst}\tilde{\mathbf{V}}_{pst}$, $\tilde{\mathbf{V}}_{pst} \in \mathbb{C}^{3L\times 3L}$ is a unitary matrix, and the diagonal elements of the diagonal matrix $\tilde{\mathbf{\Lambda}}_{pst} \in \mathbb{C}^{3L\times 3L}$ are the eigenvalues of $\mathbf{Q}(\mathbf{R}_{\text{st}}\otimes\mathbf{R}_p)\mathbf{Q}^H$. We can see that the impact of the matrix $\mathbf{Q}$ on the output SCNR has the following two aspects.

On the one hand, $\mathbf{Q}$ will influence the norm of $\tilde{\mathbf{b}}_{\text{tgt}}$, which is related to the maximum value of SCNR. On the other hand, $\mathbf{Q}$ also influences the value of $\tilde{\mathbf{b}}_{\text{tgt}}^H\tilde{\mathbf{V}}_{pst}(\tilde{\mathbf{V}}_{pst}^H\tilde{\mathbf{V}}_{pst})^{-1}\tilde{\mathbf{V}}_{pst}^H\tilde{\mathbf{b}}_{\text{tgt}}$, which is the projection of $\tilde{\mathbf{b}}_{\text{tgt}}$ into the column space of $\tilde{\mathbf{V}}_{pst}$.

Actually, the function of $\mathbf{Q}$ is to reduce the dimensionality of a complex space from a dimension of $3L$ to a dimension of L, and then we complete the distinction between clutter and target in the subspace of dimension L.

As shown in Appendix, for the single-polarimetric radar, by defining $\mathbf{R}_{\text{st}} = \mathbf{V}_{\text{st}}\mathbf{\Lambda}_{\text{st}}\mathbf{V}_{\text{st}}^H$, where $\mathbf{V}_{pst} \in \mathbb{C}^{L\times L}$ is a unitary matrix, and the diagonal elements of the diagonal matrix $\mathbf{\Lambda}_{pst} \in \mathbb{C}^{L\times L}$ are the eigenvalues of $\mathbf{R}_{\text{st}}$, we have the output SCNR denoted as

$$\text{SCNR} \approx \frac{\left|s_{hh}^{\text{tgt}}\right|^2\|\mathbf{p}_{\text{st}}\|^2}{\sigma^2}\left(1 - \frac{\mathbf{p}_{\text{st}}^H\mathbf{V}_{\text{st}}(\mathbf{V}_{\text{st}}^H\mathbf{V}_{\text{st}})^{-1}\mathbf{V}_{\text{st}}^H\mathbf{p}_{\text{st}}}{\|\mathbf{p}_{\text{st}}\|^2}\right) \tag{28}$$

where $\mathbf{p}_{\text{st}}^H\mathbf{V}_{\text{st}}(\mathbf{V}_{\text{st}}^H\mathbf{V}_{\text{st}})^{-1}\mathbf{V}_{\text{st}}^H\mathbf{p}_{\text{st}}$ represents the projection of the target into the clutter subspace in the space–time domain, and this variable is large for the low-speed target, and therefore, the output SCNR deteriorates.

Polarization optimization selects an appropriate subspace to maximize the distinction between the target and the clutter, thereby obtaining the maximum output SCNR, and we give an intuitive description in Fig. 1. In Fig. 1, we present the relative positions between two targets (represented as two 3-D vectors) in different spaces. Fig. 1 shows that two targets completely overlap in the X–Y coordinate space, and they can be distinguished in the X–Z and Y–Z coordinate spaces. Therefore, the relative positions of two 3-D vectors vary in different 2-D subspaces, and when we have to distinguish two objects in 2-D subspaces, it is necessary to select an optimal one to maximize the distinction.

The essence of element polarization selection optimization is similar to the above analysis, i.e., due to the hardware complexity of the radar system, we cannot distinguish the target from the clutter subspace in the polarization-space–time domain with dimension $3L$, and only a subspace with dimension L can be used. So, we need to choose an optimal subspace to minimize the projection of the target to the

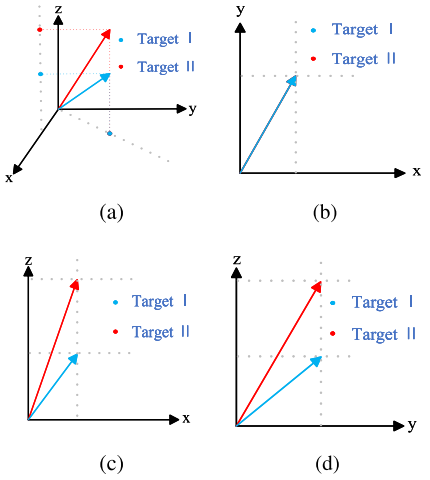

Fig. 1. Relative relationship between two targets in different spaces. (a) *X*–*Y*–*Z* coordinate. (b) *X*–*Y* coordinate. (c) *X*–*Z* coordinate. (d) *Y*–*Z* coordinate.

clutter subspace, therefore obtaining the maximum output SCNR.

It should be noticed that we use the output SCNR of adaptive filtering as the criterion for judging the performance of the proposed algorithm, and the above analysis does not consider the distribution of clutter. In fact, the statistical distribution of clutter influences the form of detectors and the characteristics of false alarm. But for adaptive filtering, we only need the CM of the clutter for the whitening filter. Therefore, the performance of polarization optimization does not depend on the distribution of clutter, but on the CM.

Polarization optimization comprehensively considers the impact of the projection of the target to the clutter subspace (i.e., $\tilde{\mathbf{b}}_{\text{tgt}}^H \tilde{\mathbf{V}}_{pst}(\tilde{\mathbf{V}}_{pst}^H \tilde{\mathbf{V}}_{pst})^{-1} \tilde{\mathbf{V}}_{pst}^H \tilde{\mathbf{b}}_{\text{tgt}}$) and the norm of the target signal (i.e., $||\tilde{\mathbf{b}}_{\text{tgt}}||$) on the output SCNR and can be achieved by solving the optimization problems (21), (22), and (25). We will discuss the solution to the above optimization problem in the next section.

B. Solution for Polarization Optimization

Note that the objective function of (26) is the function of $\mathbf{y}$ and $\mathbf{w}$, and a widely used solution approach for this problem is optimizing these two variables in a cyclic manner.

The optimal filter weights $\mathbf{w}$ can be easily obtained by (15) with $\mathbf{y}$ fixed. For a given $\mathbf{w}$, the optimization problem for $\mathbf{y}$ is the fractional quadratic programming with binary integer constraints. For this kind of problem, we can linearize the quadratic form by applying $\text{vec}(\mathbf{AXB}) = (\mathbf{B}^T \otimes \mathbf{A})\text{vec}(\mathbf{X})$, then the linear fractional model with binary integer constraints can be transformed to the problem of mixed-integer linear programming (MILP) using the method in [45], and the MILP can be solved by the optimization tools, such as GUROBI, MOSEK, CPLEX, and so on.

However, this type of solver often uses an exhaustive-like method to find the optimal solution, which requires significant computational costs. At the same time, the process of linearization will exponentially increase the dimension of the optimization variables, which increases the burden of computational complexity. Therefore, this method is only applicable when L is small, and when L is large, a more efficient solution algorithm needs to be designed.

To solve this problem, we first introduce an auxiliary variable $\mathbf{r}$, and the equivalent optimization problem is cast as

$$\begin{aligned} \min_{\mathbf{y},\mathbf{r}} \quad & \frac{\mathbf{y}^T \mathbf{\Phi}(\mathbf{w})\mathbf{y}}{\mathbf{r}^T \mathbf{\Gamma}(\mathbf{w})\mathbf{r}} \\ \text{s.t.} \quad & \mathbf{A}\mathbf{y} = \mathbf{b} \\ & \mathbf{y} = \mathbf{r} \\ & \mathbf{y} \in \{0, 1\}^{N_p L} \end{aligned} \tag{29}$$

then the scaled form of the augmented Lagrangian function of (29) is denoted by

$$\mathcal{L}_{\rho_1}(\mathbf{y}, \mathbf{r}, \mathbf{u}_1) = \frac{\mathbf{y}^T \mathbf{\Phi}(\mathbf{w})\mathbf{y}}{\mathbf{r}^T \mathbf{\Gamma}(\mathbf{w})\mathbf{r}} + \frac{\rho_1}{2}\|\mathbf{r} - \mathbf{y} + \mathbf{u}_1\|^2 \tag{30}$$

where $\mathbf{u}_1$ is the dual variable of the constraint $\mathbf{y} = \mathbf{r}$, and ρ_1 is the penalty variable that guarantees the original feasibility of $\mathbf{y} = \mathbf{r}$.

Based on the ADMM criterion, we can solve the optimization problem through the following process:

$$\mathbf{y} \leftarrow \mathcal{L}_{\rho_1}(\mathbf{y}, \mathbf{r}, \mathbf{u}_1), \text{ s.t.} \mathbf{A}\mathbf{y} = \mathbf{b}, \mathbf{y} \in \{0, 1\}^{N_p L} \tag{31a}$$

$$\mathbf{r} \leftarrow \mathcal{L}_{\rho_1}(\mathbf{y}, \mathbf{r}, \mathbf{u}_1) \tag{31b}$$

$$\mathbf{u}_1 \leftarrow \mathbf{u}_1 + \mathbf{r} - \mathbf{y}. \tag{31c}$$

Then, solutions to subproblems (31b) and (31c) will be given, respectively.

1) *Update of* $\mathbf{y}$*:* The update of $\mathbf{y}$ requires to solve the following problem:

$$\begin{aligned} \min_{\mathbf{y},\mathbf{r}} \quad & \frac{\mathbf{y}^T \mathbf{\Phi}(\mathbf{w})\mathbf{y}}{\mathbf{r}^T \mathbf{\Gamma}(\mathbf{w})\mathbf{r}} + \frac{\rho_1}{2}\|\mathbf{r} - \mathbf{y} + \mathbf{u}_1\|^2 \\ \text{s.t.} \quad & \mathbf{A}\mathbf{y} = \mathbf{b} \\ & \mathbf{y} \in \{0, 1\}^{N_p L}. \end{aligned} \tag{32}$$

With $\mathbf{r}$ fixed, we first define $\eta = 1/(\mathbf{r}^T \mathbf{\Gamma}(\mathbf{w})\mathbf{r})$, and the objective function can be casted as

$$\begin{aligned} & \frac{\mathbf{y}^T \mathbf{\Phi}(\mathbf{w})\mathbf{y}}{\mathbf{r}^T \mathbf{\Gamma}(\mathbf{w})\mathbf{r}} + \frac{\rho_1}{2}\|\mathbf{y} - (\mathbf{r} + \mathbf{u}_1)\|^2 \\ & = \eta \mathbf{y}^T \mathbf{\Phi}(\mathbf{w})\mathbf{y} \\ & \quad + \frac{\rho_1}{2}(\mathbf{y}^T\mathbf{y} - 2(\mathbf{r} + \mathbf{u}_1)^T\mathbf{y} + (\mathbf{r} + \mathbf{u}_1)^T(\mathbf{r} + \mathbf{u}_1)) \\ & = \frac{1}{2}\mathbf{y}^T(2\eta\mathbf{\Phi}(\mathbf{w}) + \rho_1 \mathbf{I}_{N_p L})\mathbf{y} \\ & \quad - \rho_1(\mathbf{r} + \mathbf{u}_1)^T\mathbf{y} + \frac{\rho_1}{2}(\mathbf{r} + \mathbf{u}_1)^T(\mathbf{r} + \mathbf{u}_1). \end{aligned} \tag{33}$$

Since $\mathbf{y}$ is a real vector, after ignoring items not related to $\mathbf{y}$, the equivalent optimization problem is denoted as

$$\begin{aligned} \min_{\mathbf{y}} \quad & \frac{1}{2}\mathbf{y}^T\mathbf{G}\mathbf{y} + \mathbf{g}^T\mathbf{y} \\ \text{s.t.} \quad & \mathbf{A}\mathbf{y} = \mathbf{b} \\ & \mathbf{y} \in \{0, 1\}^{N_pL} \end{aligned} \tag{34}$$

where $\mathbf{G} = 2\eta\mathcal{R}e\{\mathbf{\Phi}(\mathbf{w})\} + \rho_1\mathbf{I}_{N_pL}$, and $\mathbf{g} = -\rho_1(\mathbf{r} + \mathbf{u}_1)$. Therefore, the optimization problem is transformed to a real number problem.

For this binary-integer quadratic programming, we can use the method in [46] to give an effective and heuristic solution. The algorithm in [46] is based on a variation of the ADMM, and the solution is obtained by multiple iterations. In detail, each iteration of $\mathbf{y}$ consists of the following three steps:

$$\begin{aligned} \mathbf{y}^{k+1/2} = & \begin{bmatrix} \mathbf{I}_{N_pL} & \mathbf{0} \end{bmatrix} \begin{bmatrix} \mathbf{G} + \rho\mathbf{I}_{N_pL} & \mathbf{A}^T \\ \mathbf{A} & -(1/\rho)\mathbf{I}_{N_pL} \end{bmatrix}^{-1} \\ & \times \begin{bmatrix} -\mathbf{g} + \rho(\mathbf{y}^k + \mathbf{A}^T\mathbf{b} - \begin{bmatrix} \mathbf{A}^T & \mathbf{I}_{N_pL} \end{bmatrix}\mathbf{u}^k) \\ \mathbf{0} \end{bmatrix} \end{aligned} \tag{35}$$

$$\mathbf{y}^{k+1} = \Pi(\mathbf{y}^{k+1/2} + \begin{bmatrix} \mathbf{0} & \mathbf{I}_{N_pL} \end{bmatrix}\mathbf{u}^k) \tag{36}$$

and

$$\mathbf{u}^{k+1} = \mathbf{u}^k + \begin{bmatrix} \mathbf{A} \\ \mathbf{I}_{N_pL} \end{bmatrix}\mathbf{y}^{k+1/2} - \begin{bmatrix} \mathbf{0} \\ \mathbf{I}_{N_pL} \end{bmatrix}\mathbf{y}^k - \begin{bmatrix} \mathbf{b} \\ \mathbf{0} \end{bmatrix} \tag{37}$$

where $\mathbf{u}$ is the dual variable and ρ is a scalar parameter for the optimization problem (34). Moreover, $\Pi = \Pi_1 \times \Pi_2 \times \cdots \times \Pi_{N_pL}$, and Π_i, $i = 1, 2, \ldots, N_pL$, denote operators that project $\mathbf{y}(i)$ onto set $\{0, 1\}$, i.e., Π_i will approximately equal $\mathbf{y}(i)$ to 0 or 1.

This heuristic algorithm can efficiently solve the problem of mixed-integer quadratic programming. However, since the set $\{0, 1\}$ is nonconvex, and there is no guarantee that this algorithm can converge to an optimal point, this algorithm may fail to converge to a feasible point or even fail to converge. Tuning the input parameter ρ is an effective way to help the performance. Besides, we will use (35)–(37) to perform multiple iterations of $\mathbf{y}$, then we will reject $\mathbf{y}$ that satisfies $\|\mathbf{A}\mathbf{y} - \mathbf{b}\| > \varepsilon$, where ε is a tolerance for selecting the feasible points. Among the selected feasible points, we will choose the one that minimizes the objective function as the optimal $\mathbf{y}$.

2) *Update of* $\mathbf{r}$*:* To update $\mathbf{r}$, we need to solve the following optimization problem:

$$\min_{\mathbf{r}} \frac{\mu}{\mathbf{r}^T\mathbf{\Gamma}(\mathbf{w})\mathbf{r}} + \frac{\rho_1}{2}\|\mathbf{r} - \mathbf{y} + \mathbf{u}_1\|_2^2 \tag{38}$$

where $\mu = \mathbf{y}^T\mathbf{\Phi}(\mathbf{w})\mathbf{y}$. Note that the objective function of this problem is the sum of quadratic terms and fractional quadratic terms, which is an unconstrained nonconvex problem.

To solve this problem, we consider the eigendecomposition of the matrix $\mathbf{\Gamma}(\mathbf{w})$. Let $\mathbf{\Gamma}(\mathbf{w}) = \mathbf{U}\mathbf{\Lambda}\mathbf{U}^H$, where $\mathbf{U} \in \mathbb{C}^{N_pL * N_pL}$ is the unitary matrix, and $\mathbf{\Gamma}(\mathbf{w}) = \mathrm{diag}(\lambda_1, \lambda_2, \ldots, \lambda_{N_pL})$ is the diagonal matrix, whose diagonal elements are matrix eigenvalues with $\lambda_1 \geq \lambda_2 \geq \cdots \geq \lambda_{N_pL}$.

Since the matrix $\mathbf{\Gamma}(\mathbf{w})$ is a rank-one matrix, we have

$$\lambda_1 > 0, \lambda_2 = \lambda_3 = \cdots = \lambda_{N_pL} = 0. \tag{39}$$

We define $\tilde{\mathbf{r}} = \mathbf{U}^H\mathbf{r}$ and $\mathbf{v} = \mathbf{U}^H(\mathbf{y} - \mathbf{u}_1)$, and the optimization problem becomes

$$\min_{\tilde{\mathbf{r}}} \frac{\mu}{\tilde{\mathbf{r}}^H\mathbf{\Lambda}\tilde{\mathbf{r}}} + \frac{\rho_1}{2}\|\tilde{\mathbf{r}} - \mathbf{v}\|_2^2 \tag{40}$$

therefore, we have

$$\tilde{\mathbf{r}}(l) = \mathbf{v}(l), l = 2, 3, \ldots, N_pL \tag{41}$$

where $\tilde{\mathbf{r}}(l)$ is the lth element of $\tilde{\mathbf{r}}$, and $\mathbf{v}(l)$ is the lth element of $\mathbf{v}$. Then, the optimization problem becomes

$$\min_{\tilde{\mathbf{r}}(1)} \frac{\mu}{\lambda_1\tilde{\mathbf{r}}(1)^2} + \frac{\rho_1}{2}(\tilde{\mathbf{r}}(1) - \mathbf{v}(1))^2. \tag{42}$$

Then, we define $r_{1,1} = \mathcal{R}e\{\tilde{\mathbf{r}}(1)\}$, $r_{1,2} = \mathcal{I}m\{\mathbf{r}(1)\}$, $v_{1,1} = \mathcal{R}e\{\mathbf{v}(1)\}$, and $v_{1,2} = \mathcal{I}m\{\mathbf{v}(1)\}$, and thus the equivalent optimization problem of (42) is denoted by

$$\min_{r_{1,1}, r_{1,2}} \frac{\mu}{\lambda_1(r_{1,1}^2 + r_{1,2}^2)} + \frac{\rho_1}{2}(r_{1,1} - v_{1,1})^2 + \frac{\rho_1}{2}(r_{1,2} - v_{1,2})^2. \tag{43}$$

The optimality condition of this problem is

$$\begin{cases} -\frac{2\lambda_1\mu r_{1,1}}{(\lambda_1 r_{1,1}^2 + \lambda r_{1,2}^2)^2} + \rho_1(r_{1,1} - v_{1,1}) = 0 \\ -\frac{2\lambda_1\mu r_{1,2}}{(\lambda_1 r_{1,1}^2 + \lambda r_{1,2}^2)^2} + \rho_1(r_{1,2} - v_{1,2}) = 0. \end{cases} \tag{44}$$

We can easily obtain that $r_{1,1}v_{1,2} = r_{1,2}v_{1,1}$, and our discussion is divided into the following four situations according to different values of $v_{1,1}$ and $v_{1,2}$.

1) $v_{1,1} = v_{1,2} = 0$, for this case, we have

$$r_{1,1}^2 + r_{1,2}^2 = \sqrt{\frac{2\mu}{\lambda_1\rho_1}}. \tag{45}$$

At this time, we can arbitrarily generate $r_{1,1}$ and $r_{1,2}$ that meet this condition and take them as the optimal solution.

2) $v_{1,1} = 0$ and $v_{1,2} \neq 0$, for this case, we have

$$\begin{cases} r_{1,1} = 0 \\ r_{1,2}^4 - v_{1,2}r_{1,2}^3 - \frac{2\mu}{\lambda_1\rho_1} = 0. \end{cases} \tag{46}$$

The fourth-order equation in (46) can be solved directly through software, such as MATLAB, and note that we need to choose the real root that minimizes the objective function as the solution.

3) $v_{1,1} \neq 0$ and $v_{1,2} = 0$, for this case, we have

$$\begin{cases} r_{1,1}^4 - v_1r_{1,1}^3 - \frac{2\mu}{\lambda_1\rho_1} = 0 \\ r_{1,2} = 0. \end{cases} \tag{47}$$

This situation is similar to the previous one, and the optimal $r_{1,1}$ can be obtained by solving the fourth-order equation in (47).

TABLE I
Solving Process of Optimization Problem (26)

Input Parameters: $\{\rho_1, \rho\}$, $\{I_w, I_y, I_r\}$, $\mathbf{b}_{tgt}$, $\mathbf{R}_{st}$, $\mathbf{R}_p$, ϵ.

1. $i \leftarrow 0$;
2. Initialize $\mathbf{E}$, $\mathbf{T}$, $\mathbf{y}$ and $\mathbf{r}$ with the given transceiver polarization;
3. Initialize $\mathbf{A}$ and $\mathbf{b}$ according to specific issues;
4. **While** $i \leq I_w$ **do**
5. $\quad i \leftarrow i + 1$
6. $\quad$ Update $\mathbf{w}$ with (15);
7. $\quad$ Update $\mathbf{\Phi}(\mathbf{w})$ and $\mathbf{\Gamma}(\mathbf{w})$ according to specific issues;
8. $\quad$ Compute $\mathbf{\Gamma}(\mathbf{w}) \leftarrow \mathbf{U}\mathbf{\Lambda}\mathbf{U}^H$;
9. $\quad$ Compute the inverse matrix in (35);
10. $\quad$ Let $j \leftarrow 0$, $\mathbf{u}_1 \leftarrow \mathbf{0}$;
11. $\quad$ **While** $j \leq I_r$ **do**
12. $\quad\quad j \leftarrow j + 1$
13. $\quad\quad$ Calculate $\mathbf{y}_k, k = 1, 2, ..., I_y$ with (35)$\sim$(37);
14. $\quad\quad$ Find feasible $\mathbf{y}_k$ with the smallest objective value;
15. $\quad\quad \mathbf{y}_j \leftarrow \mathbf{y}_k$;
16. $\quad\quad \mathbf{v} \leftarrow \mathbf{U}^H(\mathbf{y}_j - \mathbf{u}_1)$;
17. $\quad\quad \tilde{\mathbf{r}}(l) = \mathbf{v}(l), l = 2, 3, ..., N_p L$;
18. $\quad\quad$ Calculate $r_{1,1}$ and $r_{1,2}$ by solving (43);
19. $\quad\quad \tilde{\mathbf{r}}(1) \leftarrow r_{1,1} + jr_{1,2}$ and $\mathbf{r} \leftarrow \mathbf{U}\tilde{\mathbf{r}}$;
20. $\quad\quad \mathbf{u}_1 \leftarrow \mathbf{u}_1 + \mathbf{r} - \mathbf{y}_j$;
21. $\quad$ **end**
22. $\quad$ Record $\mathbf{y}_j$ and updata $\mathbf{E}$ and $\mathbf{T}$;
23. **end**;
24. Find the feasible $\mathbf{y}$ with the smallest objective value among $\mathbf{y}_j$;
25. Outlier Processing;

Output: The optimal polarization $\mathbf{y}$;

TABLE II
Radar Parameters

Carrier frequency	1.2 GHz
Number of antenna (M)	8
Number of pulse (N)	8
Wavelength	0.25 m
PRF	2000 Hz
Platform velocity	125 m/s
Platform altitude	6000 m
Signal-to-noise ratio (SNR)	0 dB
Clutter-to-noise ratio (CNR)	40 dB

iv) $v_{1,1} \neq 0$ and $v_{1,2} \neq 0$, for this case, we have

$$\begin{cases} r_{1,1}^4 - v_{1,1} r_{1,1}^3 - \frac{2\mu v_{1,1}^4}{\lambda_1 \rho_1 (v_{1,1}^2 + v_{1,2}^2)^2} = 0 \\ r_{1,2} = \frac{v_{1,2}}{v_{1,1}} r_{1,1}. \end{cases} \tag{48}$$

Similarly, this problem can be solved in the same way. After obtaining the optimal $r_{1,1}$ and $r_{1,2}$, we have $\tilde{\mathbf{r}}(1) = r_{1,1} + jr_{1,2}$ and the optimal $\mathbf{r}$ is $\mathbf{r} = \mathbf{U}\tilde{\mathbf{r}}$.

Table I summarizes the main steps to maximize the output SCNR, where I_y refers to the iteration number for solving (34), I_r refers to the iteration number for solving (29), and I_w refers to the number of iterative update between $\mathbf{y}$ and $\mathbf{w}$. Notice that after some iterations, we select the point with the smallest objective value within the feasibility tolerance.

Moreover, the outlier processing refers to using random methods to make $\mathbf{Ay} = \mathbf{b}$, i.e., for variables that do not satisfy the equality constraints, we randomly set some variables equal to 0 or 1, so that the equality constraints hold.

In the next section, we will discuss the computational complexity and convergence of this algorithm.

C. Analysis on Computational Complexity and Convergence

1) *Computational Complexity:* From Table I, we can see that the maximization of (14) includes two loops, the inner loop is to solve the subproblem (29) through the ADMM algorithm, and the outer loop is the iterative update between $\mathbf{y}$ and $\mathbf{w}$.

For the outer loop, the main calculations include eigen-decomposition of $\mathbf{\Gamma}(\mathbf{w})$ and matrix inversion in (35), and the computational complexity is $\mathcal{O}(N_p^3 L^3)$ and $\mathcal{O}(8N_p^3 L^3)$, respectively.

For the inner loop, it includes the update of $\mathbf{y}$ and the update of $\mathbf{r}$. For the former, the computational complexity is mainly concentrated in (35), which involves matrix multiplication, and the computational complexity is $\mathcal{O}(4N_p^2 L^2)$. As for (36) and (37), they can be done much more quickly than (35) and are computationally inexpensive. As for the update of $\mathbf{r}$, the main calculation involved is unitary transformation, and the computational complexity is $\mathcal{O}(N_p^2 L^2)$.

Therefore, the computational complexity for maximizing the output SCNR is $\mathcal{O}(9N_p^3 L^3 + I_r N_p^2 L^2 + 4I_r I_y N_p^2 L^2)$.

For methods that require the use of solvers, such as Gurobi, a series of efficient heuristics and pruning techniques are used to try to find an approximately optimal solution in a reasonable time. However, it is impossible to give a definite computational complexity.

Typically, for small- to medium-sized problems, Gurobi can find high-quality solutions in a short time. For large-scale problems, it may take more time to find a better solution, and sometimes it may even not be possible to find the optimal solution in an acceptable time.

However, for large-scale problem, by reasonably setting the algorithm parameters, the proposed algorithm can quickly find an approximately optimal solution, which reflects the performance advantages of the proposed algorithm.

2) *Convergence:* Since problem (29) is NP-hard, any algorithm that finds the global solution suffers from non-polynomial worst-case runtime. Our method gives up the accuracy and uses methods that find a suboptimal solution in a short time, and the numerical results show that the proposed algorithm may fail to converge to a feasible point or even fail to converge.

Therefore, our strategy is to select the best performing point within the feasibility tolerance after multiple iterations, which may lead to outliers in the output; thus, the outlier process is added to overcome this problem. Note that the input parameters ρ_1 and ρ will influence the result, and we can improve the performance of the algorithm by tuning ρ_1 and ρ.

We point out that the output $\mathbf{y}$ may not be the global optimal solution, but it is still sufficient to improve the output SCNR.

V. SIMULATIONS

In this section, we will present simulation results for polarization optimization under different situations. We consider an airborne radar operating in the front-side-looking mode, and the parameters of the airborne radar are given in Table II; note that the signal-to-noise ratio (SNR) and clutter-to-noise ratio (CNR) in Table II correspond to the HH channel.

In our simulation, the clutter CM $\mathbf{R}_{\rm st}$ and $\mathbf{R}_p$, the scattering matrix of the target $\mathbf{S}_{\rm tgt}$, and the noise power are assumed to be known, and the influence of estimation errors is not considered. In detail, we consider the Gaussian clutter and have

$$\mathbf{R}_{\rm st} = \sum_{i=1}^{N_c} \xi_i \mathbf{p}_{{\rm st},i} \mathbf{p}_{{\rm st},i}^H \tag{49}$$

where ξ_i and $\mathbf{p}_{{\rm st},i}$ are the power and the spatial–Doppler steering vector of the ith clutter patch, respectively. The noise power is assumed to be $\sigma^2 = 0$ dB, and the power of clutter and target are set according to the preassigned SNR and CNR. Moreover, the clutter ring is divided into $N_c = 1800$ clutter patches. As for $\mathbf{R}_p$ in (12), we set $\gamma_c = \delta_c = 1$ to make the clutter power in different polarization channels the same. As for the polarization characteristics of the target in (7), we set $\mathbf{s}_{\rm tgt} = [-1j, 1.2j, 0.9]^T$ such that the SCNR of different polarization channels is different, and in detail, the SCNR of VV channel is the largest and the SCNR of HV (VH) channel is the smallest.

Then, we discuss the parameter settings of the proposed algorithm. The parameter ρ_1 corresponds to the constraint $\mathbf{y} = \mathbf{b}$, and to prevent overtightening constraints, we adjust this variable according to different target parameters. In detail, we let ρ_1 be of the same order of magnitude as the smallest eigenvalue of matrix $2\eta\mathcal{R}e\{\mathbf{\Phi}(\mathbf{w})\}$. As for the parameter ρ, we set $\rho = 2$ for the target with normalized Doppler frequency $f_d = 0$, and $\rho = 0.02$ for the target with other Doppler frequencies. Moreover, we set $I_w = 20$, $I_y = I_r = 40$, and $\epsilon = 4$.

We will give simulation results for the transmitter/receiver polarization optimization and the joint polarization optimization in the next two sections, and a detailed analysis of the simulation results is provided.

A. Results for Transmitter/Receiver Polarization Optimization

We first give simulation results for receiver polarization optimization, and the influence of different transmitter polarization and the polarization degree of clutter is demonstrated. We consider the comparison between the space–time adaptive processing (STAP) method [47], polarization space–time adaptive processing (PSTAP), and polarization optimization. The STAP corresponds to the case where both the transmitter and receiver are horizontally polarized, and the PSTAP refers to the case where

$$\mathbf{t}_l = \mathbf{e}_l = [1, 1]^T, l = 1, 2, \ldots, L \tag{50}$$

and from (27), we see that the maximum SCNR for PSTAP is $(|s_{hh}^{\rm tgt} + s_{hv}^{\rm tgt}|^2 + |s_{vv}^{\rm tgt} + s_{hv}^{\rm tgt}|^2)\|\mathbf{p}_{\rm st}\|^2/\sigma^2$, and therefore, for the high-speed target, its performance is improved compared with the single-polarization signal processing when target parameters are as mentioned above. Moreover, we can further improve the performance of PSTAP by polarization optimization [11], [14], but this issue is not considered in this article.

For the influence of transmitter polarization, we set the transmitter as horizontally polarized (i.e., $t_{h,l} = 1, l = 1, 2, \ldots, L$) in Fig. 2(a) and (c), and set the transmitter as vertically polarized (i.e., $t_{h,l} = 0, l = 1, 2, \ldots, L$) in Fig. 2(b) and (d). Simulation results show that the polarization state of the transmitter has a great impact on the results of receiver polarization optimization.

Actually, for the polarization parameter pair $(t_{h,l}, e_{h,l})$, when $t_{h,l}$ is fixed to 1 or 0, we have the parameter pair $(t_{h,l}, e_{h,l}) \in \{(1, 1), (1, 0)\}$ or $(t_{h,l}, e_{h,l}) \in \{(0, 1), (0, 0)\}$, respectively. So, according to (24), when the transmitted signal is horizontally polarized, we cannot get the data of the VV channel, which results in the inability to select polarization channels with high SCNR, and the maximum SCNR in (27) is limited. Therefore, the effect of polarization optimization is not reflected.

As for the influence of the polarization degree of clutter, we set $\rho_c = 0.9$ in Fig. 2(a) and (b) and set $\rho_c = 0.1$ in Fig. 2(c) and (d), respectively. It can be seen that when the clutter is highly polarized, the method based on PSTAP has an obvious clutter suppression effect and can also have a considerable SCNR output for low-speed targets. However, changes in parameter ρ_c have no impact on the performance of polarization optimization. This is also related to the value range of the parameter pair $(t_{h,l}, e_{h,l})$. Since $(t_{h,l}, e_{h,l}) \in \{(1, 1), (1, 0)\}$ or $(t_{h,l}, e_{h,l}) \in \{(0, 1), (0, 0)\}$, we cannot use polarization optimization to obtain the data of HH and VV channels simultaneously, and therefore, the correlation between HH and VV channels cannot be used for clutter cancellation.

It is interesting to notice that in Fig. 2(a) and (c), the output SCNR of the polarization optimization for the low-speed target is better than STAP. According to the above analysis, we see that $||\tilde{\mathbf{b}}_{\rm tgt}||^2/\sigma^2$ cannot take the maximum value, but by choosing a suitable subspace corresponding to the matrix $\mathbf{Q}$, we can change the projection of the target onto the clutter subspace, and the output SCNR is improved.

Moreover, we also present the output SCNR with random receiver polarization in Fig. 2, and we can see that even the random polarization state with the horizontally polarized transmitter will lead to SCNR improvement for the low-speed target. However, its performance is not as good as the polarization optimization, and for high-speed targets, it will even lead to performance deterioration.

Then, the simulation results for transmitter polarization optimization are presented in Fig. 3. The influence of receiver polarization and the polarization degree of clutter is also analyzed. The simulation results are similar to the previous ones. The effect of transmitter polarization optimization is affected by the polarization state of the transmitter,

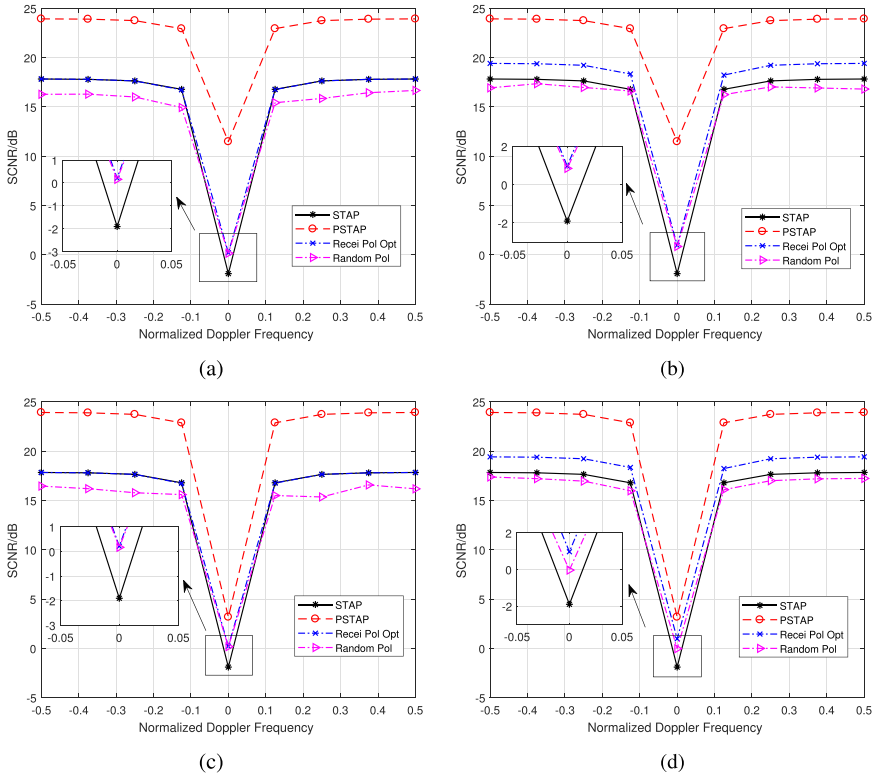

Fig. 2. Simulation results for receiver polarization optimization. (a) Horizontally polarized transmitter with $\rho_c = 0.9$. (b) Vertically polarized transmitter with $\rho_c = 0.9$. (c) Horizontally polarized transmitter with $\rho_c = 0.1$. (d) Vertically polarized transmitter with $\rho_c = 0.1$.

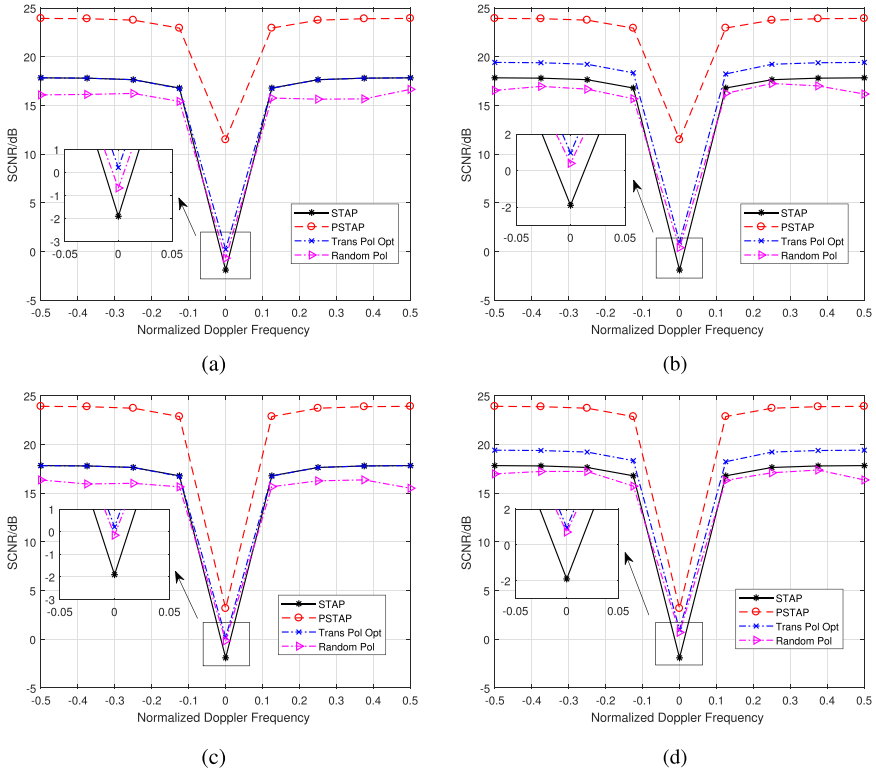

Fig. 3. Simulation results for transmitter polarization optimization. (a) Horizontally polarized receiver with $\rho_c = 0.9$. (b) Vertically polarized receiver with $\rho_c = 0.9$. (c) Horizontally polarized receiver with $\rho_c = 0.1$. (d) Vertically polarized receiver with $\rho_c = 0.1$.

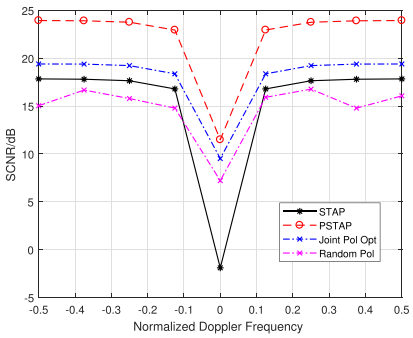

(a)

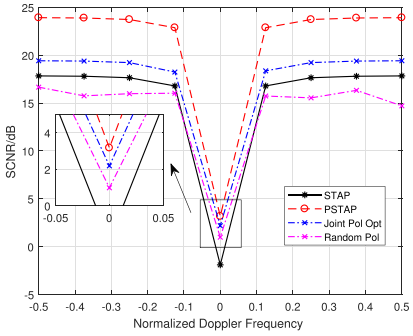

(b)

Fig. 4. Simulation results for joint polarization optimization. (a) Joint polarization optimization with $\rho_c = 0.9$. (b) Joint polarization optimization with $\rho_c = 0.1$.

and the polarization degree of clutter does not influence the performance of transmitter polarization optimization.

In fact, restricted by the polarization state of the other end, the single-end polarization optimization is to select a subspace with dimension L among 2^L complex spaces, while there are total 3^L complex spaces that meet the restrictions in (26). Therefore, the performance of the single-end polarization optimization is limited.

So far, we have analyzed the effect of transmitter/receiver polarization optimization, and we can see that the single-end polarization optimization is limited by the value range of parameters $(t_{h,l}, e_{h,l})$, and the correlation between clutter in the HH channel and VV channel cannot be used to improve the output SCNR. Therefore, it is necessary to study the joint polarization optimization of the transmitter and receiver.

B. Results for Joint Polarization Optimization

In Fig. 4, we present simulation results for joint polarization optimization. The output SCNR for targets with different normalized Doppler frequencies is presented, and the influence of the polarization degree of clutter is analyzed. It is obvious that the parameter ρ_c influences the performance of the joint polarization optimization, and even if $\rho_c = 0.1$ (i.e., the polarization degree of clutter is low), the output SCNR for the low-speed target is still improved compared to the results in Figs. 2 and 3.

It is found that this is due to the value of parameter pair $(t_{h,l}, e_{h,l})$ is no longer restricted. At this time, we have $(t_{h,l}, e_{h,l}) \in \{(1, 1), (0, 0), (1, 0), (0, 1)\}$, and therefore, we can use different antennas to receive the clutter of the HH channel and VV channel, and then the correlation of the clutter can be exploited to achieve clutter cancellation. In other words, at this time, we can choose a subspace among the 3^L complex spaces with dimension L to maximize the output SCNR, while the single-end optimization is to choose among the 2^L complex spaces.

Furthermore, for high-speed targets, the results of the joint polarization optimization are the same as the best results in Figs. 2 and 3. This is due to the maximum of $\|\mathbf{b}_{\text{tgt}}\|$ being determined when $\mathbf{s}_{\text{tgt}}$ is given; therefore, the maximum SCNR in (27) is certain.

We also give results of the random polarization, and the output SCNR of the low-speed target is improved compared to the results in Figs. 2 and 3, but the output SCNR of high-speed targets is still not good. At the same time, the performance advantage of the output SCNR obtained through polarization optimization is more obvious, which can prove the effectiveness of the proposed algorithm.

We point out that the optimal joint polarization cannot be obtained through alternating optimization of receiver polarization and transmitting polarization. This conclusion can be proved by a simple example: suppose that the optimal polarization is $(t_{h,l}, e_{h,l}) = (0, 0)$ and the initial state is $(t_{h,l}, e_{h,l}) = (1, 1)$, if the alternating optimization is used, in order to achieve the transition between these two states, we must pass through state $(t_{h,l}, e_{h,l}) = (0, 1)$ or $(t_{h,l}, e_{h,l}) = (1, 0)$, but there is no guarantee that the objective function is decreasing when the polarization state changes from $(t_{h,l}, e_{h,l}) = (1, 1)$ to $(t_{h,l}, e_{h,l}) = (0, 1)$ and from $(t_{h,l}, e_{h,l}) = (0, 1)$ to $(t_{h,l}, e_{h,l}) = (0, 0)$; therefore, we cannot use the alternating optimization to obtain the optimal joint polarization.

Based on the above simulation results, we see that the polarization optimization comprehensively considers both the maximization of the distinction between the target and clutter and the maximization of $\|\mathbf{b}_{\text{tgt}}\|$ to obtain the maximum output SCNR, and by using specific transmit–receive polarization combinations, we can achieve a better output SCNR than the single-polarimetric radar system.

Furthermore, the results in Figs. 2–4 indicate that the proposed algorithm performs worse than PSTAP. This is because PSTAP utilizes dual-polarization transmission and reception, achieving higher performance at the cost of increased hardware complexity and doubled transmitted energy. In contrast, the advantage of the proposed algorithm is that it is designed based on a radar system with lower hardware complexity, where each polarized antenna is assumed to be equipped with only one RF channel (i.e., only one polarization channel can be used for transmission and reception). Moreover, the proposed method enhances the detection of low-speed targets while maintaining the same transmitted signal energy as the single-polarimetric radar. It also reduces the computational complexity of adaptive filtering by lowering the dimensionality of the clutter CM.

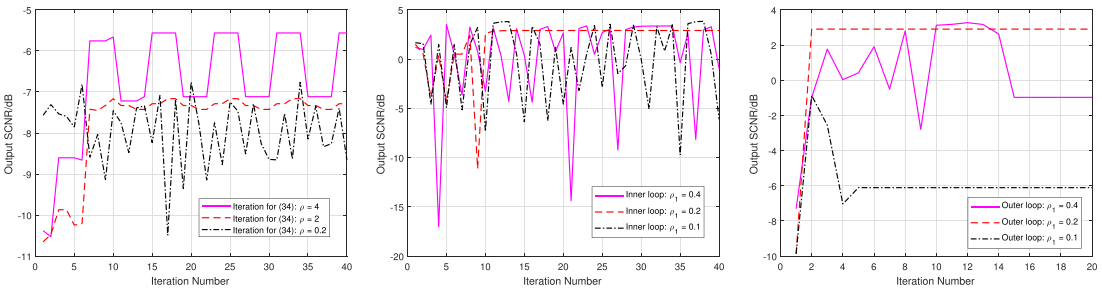

(a) (b) (c)

Fig. 5. SCNR curve with the number of iterations. (a) Iteration for problem (34). (b) Inner loop. (c) Outer loop.

Therefore, the proposed algorithm is more suitable for practical applications.

C. Convergence

In this section, we present simulation results on the convergence of the algorithm, and here, we consider the joint polarization optimization for stationary targets. First, for the subproblem (32), we use an iterative method to obtain the solution, and the SCNR curve with the number of iterations is presented in Fig. 5(a). We can see that the parameter ρ influences the result of the proposed algorithm, and the algorithm converges better with $\rho = 2$.

Then, the SCNR curve with the number of iterations for the inner loop, which refers to using the ADMM algorithm to solve the problem (29), is shown in Fig. 5(b). Moreover, the curve for the outer loop, which refers to the iterative updates between $\mathbf{w}$ and $\mathbf{s}$, is presented in Fig. 5(c). As mentioned before, the parameter ρ_1 has the same order of magnitude as the smallest eigenvalue of matrix $2\eta\mathcal{R}e\{\mathbf{\Phi}(\mathbf{w})\}$, and the inner and outer loops converge with $\rho_1 = 0.2$. So, we set $\rho = 2$ and $\rho_1 = 0.2$ in our simulation.

Unfortunately, for the results in Fig. 5, the final solution does not satisfy $\mathbf{Ay} = \mathbf{b}$, i.e., the algorithm does not converge to a feasible point. Therefore, we add some additional processing to the solutions as described in Table I. Moreover, we point out that different parameters can affect the convergence of the algorithm, and the algorithm with inappropriate parameters may even not converge at all.

D. Detection Performance

Finally, we present the detection performance of the generalized likelihood ratio test in [40] with the joint polarization obtained by the proposed algorithm. The test statistic is given by

$$\frac{\mathbf{x}^H\mathbf{R}_{\text{cn}}^{-1}\mathbf{P}(\mathbf{P}^H\mathbf{R}_{\text{cn}}^{-1}\mathbf{P})^{-1}\mathbf{P}^H\mathbf{R}_{\text{cn}}^{-1}\mathbf{x}}{1+\mathbf{x}^H\mathbf{R}_{\text{cn}}^{-1}\mathbf{x}} \underset{H_0}{\overset{H_1}{\gtrless}} \eta_0 \tag{51}$$

where H_0 hypothesis denotes the target is absent, H_1 hypothesis means the target is present, $\mathbf{P} = \mathbf{Q}(\mathbf{I}_3 \otimes \mathbf{p}_{st})$, and η_0 is the test threshold. We set the probability of false alarm $P_{\text{fa}} = 10^{-3}$, and the static target is considered in Fig. 6.

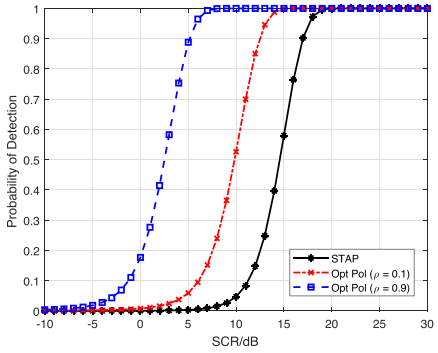

Fig. 6. Detection performance.

The curves in Fig. 6 are generated by the numerical integration method, and readers can refer to [40] and [48]. We can observe that with $K = 2L$ (i.e., the number of secondary data is twice the system degrees of freedom), the detector that exploits the optimal polarization can achieve higher detection probabilities.

In this article, our simulation experiments are based on the Gaussian clutter, and we assume that the clutter CM is known. However, in practical applications, clutter may obey a non-Gaussian distribution (such as Weibull distribution, K-distribution, generalized Pareto distribution, and so on) and the clutter CM is unknown. In this case, the key point of the proposed algorithm is to estimate the clutter CM accurately.

For the problem of CM estimation, there are various estimation methods. For example, the sample CM applies to the Gaussian clutter, and the fixed point estimation of the CM [49] is suitable for the compound Gaussian clutter, which is represented as the product of the texture component and the speckle component. Moreover, we can combine the prior structure information of the CM (such as the persymmetric structure, the Kronecker product structure, and so on) to reduce the requirement for secondary data and achieve accurate estimation of the CM in small sample cases [50]. In addition, estimation methods based on compressed sensing have also been widely used [51]. We can choose the appropriate estimation method according to the actual clutter background, and then achieve accurate CM estimation.

By using different CM estimation methods, the algorithm proposed in this article can be applied to various situations, including the heavy-tailed non-Gaussian clutter background. Since our main purpose is to analyze the influence of element polarization on clutter suppression, and we do not consider how to accurately estimate the clutter CM and the impact of CM estimation errors, we only provide simulation results based on Gaussian clutter, assuming that the clutter CM is known.

VI. CONCLUSION

In this article, motivated by the polarization sensing capabilities of the single but differently polarized antenna array and the limitations of the polarimetric radar in practical applications, we have studied the problem of element polarization selection optimization under the constraint that the polarized antenna is equipped with only one RF channel.

We first presented the transmitting–scattering–receiving process of polarized signals, and then established the signal model of the polarization-sensitive array. Moreover, the problem of polarization optimization for the transmitter (or receiver) and the problem of joint optimization of the transmitter and receiver were presented, respectively. Then, we presented a theoretical analysis of the effect of polarization optimization on the output SCNR, i.e., polarization optimization maximizes the output SCNR by selecting an appropriate subspace with dimension L in the polarization-space–time domain with dimension $3L$. Furthermore, by analyzing the optimization problem model, we have found that the abovementioned optimization problems are the fractional quadratic programming with the binary integer constraint, and then a heuristic algorithm based on the ADMM frame was proposed to find the suboptimal solution for this problem. Finally, we gave the results of polarization optimization under various scenes through simulation experiments, including the results for the transmitter (or receiver) optimization and the joint optimization of the transceiver.

Through numerical simulations, we have compared the output SCNR and detection performance (i.e., the probability of detection) of the polarization-optimized radar with the single-polarimetric radar and the dual-polarimetric radar, and the convergence of the proposed heuristic algorithm was demonstrated. We have verified that only by jointly optimizing the polarization of transmitter and receiver can the detection capability of low-speed targets be fully improved, and the heuristic algorithm needs to set appropriate input parameters, otherwise it may not converge.

It is worth noting that when we design the optimal transmitter polarization, we assume that the horizontally polarized transmitted signal has the same phase as the vertically polarized signal, which is a simplified model. In our future work, we will investigate the impact of the phase of the transmitted signal on the problem of element polarization selection optimization.

APPENDIX A
DERIVATION OF THE OUTPUT SCNR

Based on (16), and by defining $\tilde{\mathbf{b}}_{\text{tgt}} = \mathbf{Q}\mathbf{b}_{\text{tgt}}$ and $\mathbf{Q}(\mathbf{R}_{\text{st}} \otimes \mathbf{R}_p)\mathbf{Q}^H = \tilde{\mathbf{V}}_{p\text{st}}^H \tilde{\mathbf{\Lambda}}_{p\text{st}} \tilde{\mathbf{V}}_{p\text{st}}$, where $\tilde{\mathbf{V}}_{p\text{st}} \in \mathbb{C}^{3L\times 3L}$ is a unitary matrix, and the diagonal elements of the diagonal matrix $\tilde{\mathbf{\Lambda}}_{p\text{st}} \in \mathbb{C}^{3L\times 3L}$ are the eigenvalues of $\mathbf{Q}(\mathbf{R}_{\text{st}} \otimes \mathbf{R}_p)\mathbf{Q}^H$, the output SCNR can be given as

$$\begin{aligned}\text{SCNR} &= \mathbf{b}_{\text{tgt}}^H \mathbf{Q}^H (\mathbf{Q}(\mathbf{R}_{\text{st}} \otimes \mathbf{R}_p)\mathbf{Q}^H + \sigma^2 \mathbf{I}_L)^{-1} \mathbf{Q}\mathbf{b}_{\text{tgt}} \\ &= \tilde{\mathbf{b}}_{\text{tgt}}^H (\tilde{\mathbf{V}}_{p\text{st}}^H \tilde{\mathbf{\Lambda}}_{p\text{st}} \tilde{\mathbf{V}}_{p\text{st}} + \sigma^2 \mathbf{I}_L)^{-1} \tilde{\mathbf{b}}_{\text{tgt}}. \end{aligned} \tag{52}$$

By applying the matrix inversion lemma, we have

$$\begin{aligned}&\text{SCNR} \\ &= \frac{\left\|\tilde{\mathbf{b}}_{\text{tgt}}\right\|^2}{\sigma^2} - \frac{\tilde{\mathbf{b}}_{\text{tgt}}^H \tilde{\mathbf{V}}_{p\text{st}} (\tilde{\mathbf{V}}_{p\text{st}}^H \tilde{\mathbf{V}}_{p\text{st}} + \sigma^2 \tilde{\mathbf{\Lambda}}_{p\text{st}}^{-1})^{-1} \tilde{\mathbf{V}}_{p\text{st}}^H \tilde{\mathbf{b}}_{\text{tgt}}}{\sigma^2}. \end{aligned} \tag{53}$$

Since the noise power is very small compared to the clutter power, we ignore $\sigma^2 \tilde{\mathbf{\Lambda}}_{p\text{st}}^{-1}$, and the output SCNR is given by

$$\begin{aligned}&\text{SCNR} \\ &\approx \frac{\left\|\tilde{\mathbf{b}}_{\text{tgt}}\right\|^2}{\sigma^2} \left(1 - \frac{\tilde{\mathbf{b}}_{\text{tgt}}^H \tilde{\mathbf{V}}_{p\text{st}} (\tilde{\mathbf{V}}_{p\text{st}}^H \tilde{\mathbf{V}}_{p\text{st}})^{-1} \tilde{\mathbf{V}}_{p\text{st}}^H \tilde{\mathbf{b}}_{\text{tgt}}}{\left\|\tilde{\mathbf{b}}_{\text{tgt}}\right\|^2}\right). \end{aligned} \tag{54}$$

For the single-polarimetric radar, we have

$$\mathbf{Q} = \mathbf{I}_L \otimes [1, 0, 0] \tag{55}$$

and according to the previous definition, we have

$$\begin{aligned}\mathbf{Q}\mathbf{b}_{\text{tgt}} &= (\mathbf{I}_L \otimes [1, 0, 0])(\mathbf{p}_{\text{st}} \otimes \mathbf{s}_{\text{tgt}}) \\ &= s_{hh}^{\text{tgt}} \mathbf{p}_{\text{st}} \end{aligned} \tag{56}$$

and

$$\begin{aligned}&\mathbf{Q}(\mathbf{R}_{\text{st}} \otimes \mathbf{R}_p)\mathbf{Q}^H \\ &= (\mathbf{I}_L \otimes [1, 0, 0])(\mathbf{R}_{st} \otimes \mathbf{R}_p)(\mathbf{I}_L \otimes [1, 0, 0]) \\ &= \mathbf{R}_{\text{st}}. \end{aligned} \tag{57}$$

So, by defining that the eigendecomposition of $\mathbf{R}_{\text{st}}$ is $\mathbf{R}_{\text{st}} = \mathbf{V}_{\text{st}} \mathbf{\Lambda}_{\text{st}} \mathbf{V}_{\text{st}}^H$, where $\mathbf{V}_{p\text{st}} \in \mathbb{C}^{L\times L}$ is a unitary matrix, and the diagonal elements of the diagonal matrix $\mathbf{\Lambda}_{p\text{st}} \in \mathbb{C}^{L\times L}$ are the eigenvalues of $\mathbf{R}_{\text{st}}$, the output SCNR for the STAP is

$$\begin{aligned}\text{SCNR} &= \mathbf{b}_{\text{tgt}}^H \mathbf{Q}^H (\mathbf{Q}(\mathbf{R}_{\text{st}} \otimes \mathbf{R}_p)\mathbf{Q}^H + \sigma^2 \mathbf{I})^{-1} \mathbf{Q}\mathbf{b}_{\text{tgt}} \\ &\approx \frac{\left|s_{hh}^{\text{tgt}}\right|^2 \|\mathbf{p}_{\text{st}}\|^2}{\sigma^2} \left(1 - \frac{\mathbf{p}_{\text{st}}^H \mathbf{V}_{\text{st}} (\mathbf{V}_{\text{st}}^H \mathbf{V}_{\text{st}})^{-1} \mathbf{V}_{\text{st}}^H \mathbf{p}_{\text{st}}}{\|\mathbf{p}_{\text{st}}\|^2}\right). \end{aligned} \tag{58}$$

The derivation of (58) uses the same method as the derivation of (54).

REFERENCES

[1] D. Giuli, "Polarization diversity in radars," *Proc. IEEE*, vol. 74, no. 2, pp. 245–269, Feb. 1986.

[2] X. Yuan, "Estimating the DOA and the polarization of a polynomial-phase signal using a single polarized vector-sensor," *IEEE Trans. Signal Process.*, vol. 60, no. 3, pp. 1270–1282, Mar. 2012.

[3] K. T. Wong and M. D. Zoltowski, "Uni-vector-sensor ESPRIT for multisource azimuth, elevation, and polarization estimation," *IEEE Trans. Antennas Propag.*, vol. 45, no. 10, pp. 1467–1474, Oct. 1997.

[4] Y. Xu, Z. Liu, K. T. Wong, and J. Cao, "Virtual-manifold ambiguity in HOS-based direction-finding with electromagnetic vector-sensors," *IEEE Trans. Aerosp. Electron. Syst.*, vol. 44, no. 4, pp. 1291–1308, Oct. 2008.

[5] K. T. Wong and X. Yuan, ""Vector cross-product direction-finding" with an electromagnetic vector-sensor of six orthogonally oriented but spatially noncollocating dipoles/loops," *IEEE Trans. Signal Process.*, vol. 59, no. 1, pp. 160–171, Jan. 2011.

[6] B. C. R. Bakker, "McMaster IPIX radar sea clutter database," 1998. [Online]. Available: http://soma.mcmaster.ca/ipix.php

[7] G. Jian et al., "Sea-detecting radar experiment and target feature data acquisition for dual polarization multistate scattering dataset of marine targets," *J. Radar*, vol. 12, no. 2, pp. 456–469, 2023.

[8] K. T. Wong and M. D. Zoltowski, "Self-initiating MUSIC-based direction finding and polarization estimation in spatio-polarizational beamspace," *IEEE Trans. Antennas Propag.*, vol. 48, no. 8, pp. 1235–1245, Aug. 2000.

[9] Y. Hua, "A pencil-MUSIC algorithm for finding two-dimensional angles and polarizations using crossed dipoles," *IEEE Trans. Antennas Propag.*, vol. 41, no. 3, pp. 370–376, Mar. 1993.

[10] J. Li and R. Compton, "Angle and polarization estimation using ESPRIT with a polarization sensitive array," *IEEE Trans. Antennas Propag.*, vol. 39, no. 9, pp. 1376–1383, Sep. 1991.

[11] J.-J. Xiao and A. Nehorai, "Joint transmitter and receiver polarization optimization for scattering estimation in clutter," *IEEE Trans. Signal Process.*, vol. 57, no. 10, pp. 4142–4147, Oct. 2009.

[12] H. Dai, X. Wang, Y. Li, Y. Liu, and S. Xiao, "Main-lobe jamming suppression method of using spatial polarization characteristics of antennas," *IEEE Trans. Aerosp. Electron. Syst.*, vol. 48, no. 3, pp. 2167–2179, Jul. 2012.

[13] G. A. Showman, W. Melvin, and M. Belenkii, "Performance evaluation of two polarimetric STAP architectures," in *Proc. IEEE Radar Conf.*, 2003, pp. 59–65.

[14] L. Xie, Z. He, J. Tong, J. Li, and H. Li, "Transmitter polarization optimization for space-time adaptive processing with diversely polarized antenna array," *Signal Process.*, vol. 169, 2020, Art. no. 107401.

[15] L. M. Novak, M. B. Sechtin, and M. J. Cardullo, "Studies of target detection algorithms that use polarimetric radar data," *IEEE Trans. Aerosp. Electron. Syst.*, vol. 25, no. 2, pp. 150–165, Mar. 1989.

[16] H.-R. Park, J. Li, and H. Wang, "Polarization-space-time domain generalized likelihood ratio detection of radar targets," *Signal Process.*, vol. 41, no. 2, pp. 153–164, 1995.

[17] L. Novak, M. Burl, and W. Irving, "Optimal polarimetric processing for enhanced target detection," *IEEE Trans. Aerosp. Electron. Syst.*, vol. 29, no. 1, pp. 234–244, Jan. 1993.

[18] M. Hurtado and A. Nehorai, "Polarimetric detection of targets in heavy inhomogeneous clutter," *IEEE Trans. Signal Process.*, vol. 56, no. 4, pp. 1349–1361, Apr. 2008.

[19] A. D. Maio, G. Alfano, and E. Conte, "Polarization diversity detection in compound-Gaussian clutter," *IEEE Trans. Aerosp. Electron. Syst.*, vol. 40, no. 1, pp. 114–131, Jan. 2004.

[20] D. Pastina, P. Lombardo, and T. Bucciarelli, "Adaptive polarimetric target detection with coherent radar. I. Detection against Gaussian background," *IEEE Trans. Aerosp. Electron. Syst.*, vol. 37, no. 4, pp. 1194–1206, Oct. 2001.

[21] F. Colone and F. Filippini, "Autoregressive model based polarimetric adaptive detection scheme Part I: Theoretical derivation and performance analysis," *IEEE Trans. Aerosp. Electron. Syst.*, vol. 56, no. 5, pp. 3762–3778, Oct. 2020.

[22] F. Colone and F. Filippini, "Autoregressive model based polarimetric adaptive detection scheme Part II: Performance assessment under spectral model mismatch," *IEEE Trans. Aerosp. Electron. Syst.*, vol. 56, no. 5, pp. 3779–3795, Oct. 2020.

[23] Z. Wang, Z. He, Q. He, B. Xiong, and Z. Cheng, "Persymmetric adaptive target detection with dual-polarization in compound Gaussian sea clutter with inverse gamma texture," *IEEE Trans. Geosci. Remote Sens.*, vol. 60, 2022, Art. no. 5118117.

[24] S. R. Cloude and E. Pottier, "A review of target decomposition theorems in radar polarimetry," *IEEE Trans. Geosci. Remote Sens.*, vol. 34, no. 2, pp. 498–518, Mar. 1996.

[25] S. Bickel, "Some invariant properties of the polarization scattering matrix," *Proc. IEEE*, vol. 53, no. 8, pp. 1070–1072, Aug. 1965.

[26] P. Ferrazzoli, L. Guerriero, and G. Schiavon, "Experimental and model investigation on radar classification capability," *IEEE Trans. Geosci. Remote Sens.*, vol. 37, no. 2, pp. 960–968, Mar. 1999.

[27] N. E. Chamberlain, E. K. Walton, and F. D. Garber, "Radar target identification of aircraft using polarization-diverse features," *IEEE Trans. Aerosp. Electron. Syst.*, vol. 27, no. 1, pp. 58–67, Jan. 1991.

[28] S. R. Cloude and E. Pottier, "Concept of polarization entropy in optical scattering," *Opt. Eng.*, vol. 34, no. 6, pp. 1599–1610, 1995.

[29] V. Karnychev, V. A. Khlusov, L. P. Ligthart, and G. Sharygin, "Algorithms for estimating the complete group of polarization invariants of the scattering matrix (SM) based on measuring all SM elements," *IEEE Trans. Geosci. Remote Sens.*, vol. 42, no. 3, pp. 529–539, Mar. 2004.

[30] K. Sarabandi and F. Ulaby, "A convenient technique for polarimetric calibration of single-antenna radar systems," *IEEE Trans. Geosci. Remote Sens.*, vol. 28, no. 6, pp. 1022–1033, Nov. 1990.

[31] E. Gorgucci, G. Scarchilli, and V. Chandrasekar, "Calibration of radars using polarimetric techniques," *IEEE Trans. Geosci. Remote Sens.*, vol. 30, no. 5, pp. 853–858, Sep. 1992.

[32] K. Sarabandi, F. T. Ulaby, and M. A. Tassoudji, "Calibration of polarimetric radar systems with good polarization isolation," *IEEE Trans. Geosci. Remote Sens.*, vol. 28, no. 1, pp. 70–75, Jan. 1990.

[33] Y. Wang and V. Chandrasekar, "Polarization isolation requirements for linear dual-polarization weather radar in simultaneous transmission mode of operation," *IEEE Trans. Geosci. Remote Sens.*, vol. 44, no. 8, pp. 2019–2028, Aug. 2006.

[34] R. Touzi, P. W. Vachon, and J. Wolfe, "Requirement on antenna cross-polarization isolation for the operational use of C-band SAR constellations in maritime surveillance," *IEEE Geosci. Remote Sens. Lett.*, vol. 7, no. 4, pp. 861–865, Oct. 2010.

[35] B. Li, Y.-Z. Yin, W. Hu, Y. Ding, and Y. Zhao, "Wideband dual-polarized patch antenna with low cross polarization and high isolation," *IEEE Antennas Wireless Propag. Lett.*, vol. 11, pp. 427–430, 2012.

[36] M. Costa, A. Richter, and V. Koivunen, "Unified array manifold decomposition based on spherical harmonics and 2-D Fourier basis," *IEEE Trans. Signal Process.*, vol. 58, no. 9, pp. 4634–4645, Sep. 2010.

[37] M. Costa, A. Richter, and V. Koivunen, "DoA and polarization estimation for arbitrary array configurations," *IEEE Trans. Signal Process.*, vol. 60, no. 5, pp. 2330–2343, May 2012.

[38] M. Dai, X. Ma, W. Sheng, and Y. Han, "Linear dipole array with element rotation for enhanced DOA and polarization estimation," *IEEE Trans. Aerosp. Electron. Syst.*, vol. 59, no. 6, pp. 9128–9141, Dec. 2023.

[39] Y. Yue, C. Zhou, F. Xing, K.-K. R. Choo, and Z. Shi, "Adaptive beamforming for cascaded sparse diversely polarized planar array," *IEEE Trans. Veh. Technol.*, vol. 72, no. 12, pp. 15648–15664, Dec. 2023.

[40] J. Wang, Y. Wang, Z. Wang, Z. He, and B. Xiong, "Polarization-space-time domain adaptive detection for the heterogeneous array," *Signal Process.*, vol. 210, 2023, Art. no. 109094.

[41] G. Sinclair, "The transmission and reception of elliptically polarized waves," *Proc. IRE*, vol. 38, no. 2, pp. 148–151, Feb. 1950.

[42] S. Nghiem, S. Yueh, R. Kwok, and F. Li, "Symmetry properties in polarimetric remote sensing," *Radio Sci.*, vol. 27, no. 05, pp. 693–711, Sep./Oct. 1992.

[43] L. Pallotta, C. Clemente, A. D. Maio, and J. J. Soraghan, "Detecting covariance symmetries in polarimetric SAR images," *IEEE Trans. Geosci. Remote Sens.*, vol. 55, no. 1, pp. 80–95, Jan. 2017.

[44] L. Pallotta, A. D. Maio, and D. Orlando, "A robust framework for covariance classification in heterogeneous polarimetric SAR images and its application to L-band data," *IEEE Trans. Geosci. Remote Sens.*, vol. 57, no. 1, pp. 104–119, Jan. 2019.

[45] A. Charnes and W. W. Cooper, "Programming with linear fractional functionals," *Nav. Res. Logistics Quart.*, vol. 9, no. 3/4, pp. 181–186, 1962.

[46] R. Takapoui, N. Moehle, S. Boyd, and A. Bemporad, "A simple effective heuristic for embedded mixed-integer quadratic programming," *Int. J. Control*, vol. 93, no. 1, pp. 2–12, 2020.

[47] J. Ward, "Space-time adaptive processing for airborne radar," *MIT Lincoln Lab.*, Lexington, MA, USA, Tech. Rep. 1015, Dec. 1998.

[48] E. J. Kelly, "An adaptive detection algorithm," *IEEE Trans. Aerosp. Electron. Syst.*, vol. AES-22, no. 2, pp. 115–127, Mar. 1986.

[49] D. E. Tyler, "A distribution-free M-estimator of multivariate scatter," *Ann. Statist.*, vol. 15, pp. 234–251, 1987.

[50] Y. Sun, P. Babu, and D. P. Palomar, "Robust estimation of structured covariance matrix for heavy-tailed elliptical distributions," *IEEE Trans. Signal Process.*, vol. 64, no. 14, pp. 3576–3590, Jul. 2016.

[51] A. Gilbert and P. Indyk, "Sparse recovery using sparse matrices," *Proc. IEEE*, vol. 98, no. 6, pp. 937–947, Jun. 2010.